Advances in Differential Equations and Control Processes 2026, 33(2), 4147.
doi: https://doi.org/10.59400/adecp4147

Article

Effect of heater location and wall waviness on buoyant convection in a porous wavy cavity using heat function approach

Huey Tyng Cheong[1] , **Sivasankaran Sivanandam**[2,3,*]

[1] School of Mathematical Sciences, Sunway University, Sunway City 47500, Malaysia

[2] Department of Mathematics, King Abdulaziz University, Jeddah 21589, Saudi Arabia

[3] Department of Mathematics, Saveetha School of Engineering, Saveetha Institute of Medical and Technical Sciences (SIMATS), Chennai 602105, India

*** Corresponding authors:** Sivasankaran Sivanandam, sd.siva@yahoo.com

CITATION

Cheong HT, Sivanandam S. Effect of heater location and wall waviness on buoyant convection in a porous wavy cavity using heat function approach. Advances in Differential Equations and Control Processes. 2026; 33(2): 4147.
https://doi.org/10.59400/adecp4147

ARTICLE INFO

Received: 10 March 2026
Revised: 13 April 2026
Accepted: 17 April 2026
Available online: 30 April 2026

Abstract: Natural convection and thermal transport in a porous square cavity with a wavy cold wall and a localized heat source on the left sidewall are numerically examined in this work. The cavity is filled with a fluid-saturated porous medium and is governed by the Darcy model under steady, laminar flow conditions with the Boussinesq approximation. A heater of fixed length is mounted on the left sidewall at three different points, namely the lower, center, and upper positions, while the right sidewall is maintained at a constant cold temperature and modeled with varying waviness in terms of amplitude and number of undulations. The remaining walls are considered adiabatic. The governing dimensionless equations for energy and stream functions are discretized using the finite difference technique and solved iteratively for various heater positions, right sidewall waviness, and Darcy–Rayleigh values after transforming the physical wavy domain into a rectangular computational domain. Results are presented in the form of Nusselt numbers, isotherms, streamlines, and heatlines. The findings indicate that the heater position has a significant influence on the convection flow, and heat transfer performance. The averaged heat transmission rate is improved by the right sidewall's increased waviness. Among the heater placements, lower heating produces the highest averaged heat transfer for higher Darcy–Rayleigh numbers, whereas center heating is more effective under weak convection conditions. This study provides useful insight into the thermal design of porous systems involving non-uniform heating, such as solar air conditioning, ventilation, and heating systems.

Keywords: heat function; natural convection; wavy cavity; porous medium; localized heating

1. Introduction

The natural convective current and thermal transport through porous media have been the subject of much research in recent decades because of their numerous uses in geothermal technology, biomedical science, energy engineering, and other fields, see Upreti et al. [1]. Numerous research and concepts on convective stream and thermal energy transfer through porous media were also supplied by Upreti et al. [1] and Sharma et al. [2]. For modeling technical challenges like solar energy collectors, geothermal reservoirs, and cooking appliances, cavities with uneven walls may be more realistic. Murthy et al. [3] inspected buoyant convective currents in a Darcy porous chamber with an isothermally heated bottom wavy wall. Then, using the Forchheimer-extended

Darcy model, Rathish Kumar and Shalini [4] examined convective stream and heat transfer in a porous hollow with an isothermally heated left wavy wall. Both discovered that the rate of heat transfer into the domain is decreased by a heated, wavy wall. Das et al. [5] investigated an in-phase wavy chamber with horizontal wavy walls. The natural convection mechanism in an in-phase wavy porous cavity with vertical wavy walls was then explored by Misirlioglu et al. [6] and Chen et al. [7]. Under the impact of thermal radiation, Mansour et al. [8] examined a wavy porous cavity that was heated on both the top and bottom wavy walls. Using the Darcy model, Sojoudi et al. [9] achieved a numerical investigation on free convective current in a chamber with thermally active in-phase wavy left and right walls. They determined that the alteration in amplitude disturbs the stream, whereas the undulation number affects the stream pattern along the wall(s).

Magnetohydrodynamic (MHD) buoyant convection in a partially open wavy chamber filled with nanofluid saturated porous matrix was studied by Prakash et al. [10]. They discovered that when the nanoparticle volume percentage or Hartmann number rises, overall convection falls, and waviness raises the averaged Nusselt number. The stream and heat transport were scrutinised by Armaghani et al. [11] in a hybrid nanofluid-filled porous enclosure with wavy walls. They detected that the averaged Nusselt number of hybrid nanofluids rises with increasing volume fraction. Heat transmission in a wavy cavity with MHD and nonlinear mixed convection was examined by Tanveer et al. [12]. They found that heat increases as it gets closer to the upper wall under the influence of the volume fraction parameter and the Hartman number. The impact of an angled magnetic field on entropy formation in double-diffusive natural convection flow in a wavy enclosure containing a non-Newtonian Casson fluid was investigated by Chuhan et al. [13]. In a wavy porous cavity, Mandal et al. [14] considered non-uniform multi-frequency heating with a hybrid nanoliquid and a magnetic field. They observed that the increased undulation height on the wavy sidewalls improved the heat transfer. Free convective stream and energy transport in a tilted hollow filled with porous material were inspected by Sivasankaran et al. [15]. They found that the oblique cavity had a higher amount of heat transport than the vertical square cavity.

Hansda et al. [16] studied the magneto-double diffusion convective current in a porous wavy cavity holding a radiative hybrid nanoliquid. They asserted that hybrid nanoparticles are responsible for enhancing energy transmission and decreasing solute transfer, and that the small heater produces the highest values of thermo-solutal transfer. Parmar et al. [17] created a novel fractional order double-diffusion model to investigate the solute transport phenomena, convective heat, and the transitory nature of fluid flow within a wavy porous cavity. As the values of the fractional order parameters increase, the evolution rate is observed to accelerate. Barman and Kumar [18] investigated entropy formation in the convective current of a hybrid nanoliquid in a partially heated wavy non-Darcy porous inclined chamber. They found that the Bejan number is increased by both the hybridised nanoliquid and the inertial effect. In a trapezoidal container with wavy sidewalls, Roy et al. [19] investigate the natural convective stream of a ternary hybrid nanoliquid. They discovered that the averaged Nusselt number

increases with raising the Rayleigh number and the sloped wall angle of the trapezium.

The thermally active wall would have an uneven temperature distribution if it were shaded or had a heat-conducting substance on it. Therefore, it is crucial to investigate how non-uniform heating affects temperature-dependent electronics because it may have an impact on the devices' overall performance. Sankar et al. [20] quantitatively examined the effects of five distinct pairings of partial cooling/heating locations on the corresponding left and right walls of a square porous hollow. The average Nusselt number is found to be highest in the midway cooling and heating scenario. Next, magneto-convection inside a square cavity with nine dissimilar pairs of cool/hot locations on the left/right walls, respectively, was investigated by Sivasankaran and Bhuvaneswari [21]. They found that heat transfer is improved when the cooler is positioned at the top or center part, and the heater is positioned at the middle or bottom. The impact of partial heating on a square cavity's left and bottom walls was inspected by Chen and Chen [22]. They discovered that two small heaters on the bottom walls and a long heater in the top-left position increase the rate of heat transfer. Doubly diffusive convective current in a porous chamber with varied heating locations on the right wall was investigated by Zhao et al. [23, 24]. When the heater is positioned higher on the right wall, it is found that the averaged Nusselt number is small.

Several studies have used computational methods to examine the impact of discontinuous heating on mixed convective currents in a lid-moving chamber [25–27]. The convective current in a rectangular-shaped porous chamber with two iso-flux heat sources on the left sidewall was inspected by Sivasankaran et al. [25]. It is discovered that the bottom heat source has a higher average heat transport rate than the top heat source. Heat transmission is improved when a shorter heater is utilized in mixed convection inside a lid-moving chamber, according to Sivakumar et al. [26]. In the occurrence of a magnetic field, middle heating results in a higher average heat transfer rate, according to Malleswaran et al. [27]. According to Sivasankaran et al. [28] and Malleswaran and Sivasankaran [29], when the horizontal heater is longer than the vertical heater, the average heat transfer rate is higher. Buoyant convection in cavities with different kinds and positions of heaters was briefly reviewed by Öztop et al. [30]. A porous, wavy hollow with an open top wall was recently examined by Rao and Barman [31], who concluded that the aperture lessens the impact of the wavy wall.

There isn't much research on buoyant convective currents in a porous wavy chamber with localized heating, according to a thorough study of the literature. To address this gap, the current research examines heat diffusion and spontaneous convection currents in a porous wavy cavity with a localized heat source on the left sidewall. The primary focus of this investigation will be the sidewall's waviness and heating positions on the flow structure and thermal behavior. The resulting hydrodynamic and thermal fields are illustrated using streamline, isotherm, and heatline contours to provide detailed physical insight into the transfer mechanics. In addition, the heat transfer performance of the cavity is quantified through local and average Nusselt numbers under varying governing parameters. The outcomes of this study are expected to enhance the understanding of localized thermal actuation in complex porous

geometries and to provide useful guidance for the thermal design of passive energy and heat management systems.

2. Materials and methods

Figure 1 illustrates the physical domain of the current study along with the boundary conditions. The velocities u and v are taken in the route of the x- and y-axes, respectively.

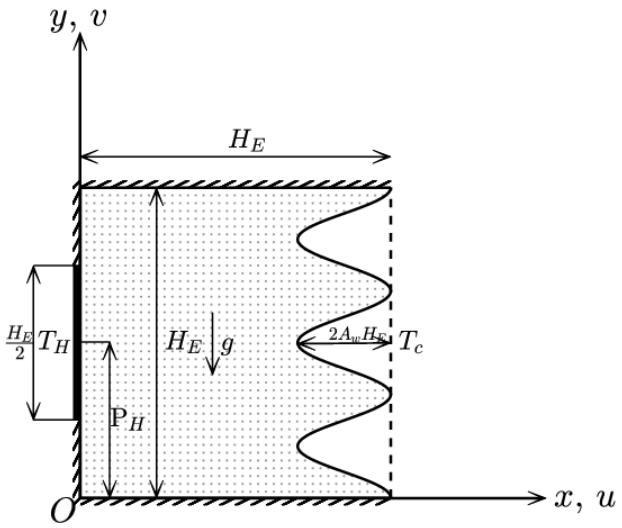

Figure 1. Schematic diagram.

A 2D square cavity of width and height H_E filled with a fluid-saturating porous medium is considered. The right wall of the cavity is a wavy surface with an undulation number (λ_w) and amplitude (A_w). A constant size of the heater ($H_E/2$) is placed on the left wall at a temperature T_H, while the wavy right wall is chilled at T_c ($T_H > T_c$). The heater is placed at three locations on the left sidewall, namely, lower, center, and upper. The heater position (P_H) is measured from the left wall's bottom edge to the center of the heat source. Hence, the heater positions on the left wall are $\frac{H_E}{4}$ (lower), $\frac{H_E}{2}$ (center), and $\frac{3H_E}{4}$ (upper), respectively. Adiabatic conditions are imposed on the remaining areas of the left sidewall and the horizontal barriers of the cavity. The gravity, g, acts vertically downward. The fluid is Newtonian and incompressible. Also, fluid properties are not varying, except in the buoyant term, where the fluid density is expressed as a linear function of temperature, by the Boussinesq approximation [32]. The stream is presumed to be steady, laminar, and viscous dissipation is insignificant. The Darcy model-based porous matrix is presumed to be isotropic, homogeneous, and in thermal equilibrium with the local fluid [33]. Based on the laws of conservation, the governing model equations are:

$$\frac{\partial u}{\partial x} + \frac{\partial v}{\partial y} = 0, \tag{1}$$

$$u = -\frac{K}{\mu}\frac{\partial P}{\partial x}, \tag{2}$$

$$v = -\frac{K}{\mu}\frac{\partial P}{\partial y} + \frac{K}{\mu}\beta g\rho\left(T - T_c\right), \tag{3}$$

$$u\frac{\partial T}{\partial x}+v\frac{\partial T}{\partial y}=\frac{k}{\rho c_P}\left(\frac{\partial^2 T}{\partial x^2}+\frac{\partial^2 T}{\partial y^2}\right), \tag{4}$$

where K is the permeability of the porous medium, μ is the fluid viscosity, P is the pressure, β is the thermal expansion coefficient, ρ is the fluid density, k is the thermal conductivity, and c_P is the specific heat of the fluid at constant pressure.

Based on the above-mentioned arrangements of the model, the boundary values of the cavity are:

on walls (all):

$$u=v=0, \tag{5a}$$

on $x=0$, $(\mathrm{P}_H-\frac{H_E}{4})\leq y\leq(\mathrm{P}_H+\frac{H_E}{4})$:

$$T=\ T_H, \tag{5b}$$

on $x=H_E-A_wH_E+A_wH_E\cos\left(2\pi\lambda_w\frac{y}{H_E}\right), 0\leq y\leq H_E$:

$$T=\ T_c, \tag{5c}$$

on $x=0, 0<y<(P_H-H_E/4)$ & $(P_H+H_E/4)\ <y<H_E$:

$$\frac{\partial T}{\partial x}=0, \tag{5d}$$

on $y=0$ & $H_E, 0\leq x\leq H_E$:

$$\frac{\partial T}{\partial y}=0. \tag{5e}$$

where $P_H\ =\ H_E/4, H_E/2, 3H_E/4$ for the case of the lower, center, and upper positions of the heat source, respectively. Heatlines are useful for the visualization of the heat transport process inside the porous domain. The heat function for the buoyant current inside the porous cavity is given by:

$$-\frac{\partial h}{\partial x}=\rho c_P v(T-T_c)-k\frac{\partial T}{\partial y}, \tag{6}$$

$$\frac{\partial h}{\partial x}=\rho c_P u(T-T_c)-k\frac{\partial T}{\partial x}, \tag{7}$$

where h is the heat function, which is assumed to be a continuous function with its second-order derivatives. Taking x- and y-derivatives, respectively, of Equations (6) and (7) gives:

$$\frac{\partial^2 h}{\partial x^2}+\frac{\partial^2 h}{\partial y^2}=\rho c_P\left[\left(-v\frac{\partial T}{\partial x}+u\frac{\partial T}{\partial y}\right)+(T-T_c)\left(\frac{\partial u}{\partial y}-\frac{\partial v}{\partial x}\right)\right]. \tag{8}$$

The heat function for the inner region of the porous domain is governed by Equation (8). The boundary values of the heat function are obtained from Equations (6) and (7) when the velocity components are zero along the solid walls.

on $y = 0$ & H_E, $0 \leq x \leq\ H_E$:

$$h(x,y) = h(0,y) - k\int_0^x \frac{\partial T}{\partial y}\quad \mathrm{d}x, \tag{9a}$$

on $x = 0$ & $H_E - A_w H_E + A_w H_E \cos\left(2\pi\lambda_w \frac{y}{H_E}\right),\ 0 \leq y \leq H_E$:

$$h(x,y) = h(x,0) - k\int_0^s \frac{\partial T}{\partial n}\quad \mathrm{d}s, \tag{9b}$$

where s and n are respectively the tangent and normal of the sidewall being measured, i.e., $n = x$ and $s = y$ for the left wall calculation.

The heat transmission rate across the cavity is a vital measurement in determining the significance of the model proposed in this study. Henceforth, the local heat transference at any point on the side walls (q) and the averaged heat transfer amount ($\bar{q}$) are calculated as:

$$q = -k\frac{\partial T}{\partial n}, \tag{10}$$

$$\bar{q} = \frac{2}{H_E}\int_{P_H - H_E/4}^{P_H + H_E/4} q\ \ \mathrm{d}y. \tag{11}$$

The stream function is found by removing the pressure terms in the respective y- and x-derivatives of the momentum Equations (2) and (3), and then the velocities are provided as follows:

$$u = \frac{\partial \psi}{\partial y},\ \ v = -\frac{\partial \psi}{\partial x}. \tag{12}$$

To scale the dimensional model into dimensionless form, dimensionless variables are added. By using this procedure, the system of equations can be solved with fewer variables, including dimensional physical quantities. Therefore, the dimensionless quantities listed below are used in this study:

$$\begin{aligned} (X,Y) &= \tfrac{(x,y)}{H_E},\ \ \Theta = \tfrac{T - T_c}{T_H - T_c},\ \ \Psi = \tfrac{\psi}{\alpha}, \\ H &= \tfrac{h}{k(T_H - T_c)},\ \ Ra_D = \tfrac{K\beta h(T_H - T_c)H_E}{\alpha \upsilon}, \end{aligned} \tag{13}$$

where Ra_D is the Darcy-Rayleigh number based on the height of the cavity H_E.

The dimensionless governing model is as follows, after the dimensionless variables (13) are substituted into the governing Equations (1)–(4) and boundary conditions (5):

$$\frac{\partial^2 \Psi}{\partial X^2} + \frac{\partial^2 \Psi}{\partial Y^2} = -Ra_D \frac{\partial \Theta}{\partial X}, \tag{14}$$

$$\frac{\partial^2 \Theta}{\partial X^2} + \frac{\partial^2 \Theta}{\partial Y^2} = \frac{\partial \Psi}{\partial Y}\frac{\partial \Theta}{\partial X} - \frac{\partial \Psi}{\partial X}\frac{\partial \Theta}{\partial Y}, \tag{15}$$

with appropriate boundary values,

on walls:

$$\Psi = 0, \tag{16a}$$

on $X = 0$, $(P_H/H_E - \frac{1}{4}) \leq Y \leq (P_H/H_E + \frac{1}{4})$:

$$\Theta = 1, \tag{16b}$$

on $X = 1 - A_w + A_w \cos(2\lambda_w \pi Y)$, $0 \leq Y \leq 1$:

$$\Theta = 0, \tag{16c}$$

on $X = 0$, $0 < Y < \left(\frac{P_H}{H_E} - \frac{1}{4}\right)$ & $(P_H/H_E + \frac{1}{4}) < Y < 1$:

$$\frac{\partial \Theta}{\partial X} = 0, \tag{16d}$$

on $Y = 0$ & 1, $0 \leq X \leq 1$:

$$\frac{\partial \Theta}{\partial Y} = 0. \tag{16e}$$

where $P_H/H_E = 1/4,\ 1/2$ and $3/4$ are lower, center and upper heating, respectively.

The dimensionless heat function will be:

$$\frac{\partial^2 H}{\partial X^2} + \frac{\partial^2 H}{\partial Y^2} = \left(\frac{\partial \Psi}{\partial X}\frac{\partial \Theta}{\partial X} + \frac{\partial \Psi}{\partial Y}\frac{\partial \Theta}{\partial Y}\right) + \Theta\left(\frac{\partial^2 \Psi}{\partial X^2} + \frac{\partial^2 \Psi}{\partial Y^2}\right), \tag{17}$$

with boundary values,

on $Y = 0$ & 1, $0 \leq X \leq 1$:

$$H(X,\ Y) = H(0, Y) - \int_0^X \frac{\partial \Theta}{\partial Y} \ \mathrm{d}X, \tag{18a}$$

on $X = 0$ & $1 - A_w + A_w \cos(2\lambda_w \pi Y)$, $0 \leq Y \leq 1$:

$$H(X, Y) = H(X, 0) - \int_0^S \frac{\partial \Theta}{\partial N} \ \mathrm{d}S, \tag{18b}$$

where $S = s/L$ and $N = n/L$ are tangent and normal to the sidewall, respectively.

The heat transfer amount is computed by the Nusselt number. The local Nusselt number (Nu) at any location on the sidewalls, and the averaged Nusselt number of the heater are computed as follows:

$$Nu = -\frac{\partial \Theta}{\partial N}, \tag{19}$$

$$\overline{Nu} = 2\int_{P_H/H_E - 1/4}^{P_H/H_E + 1/4} Nu \quad \mathrm{d}Y. \tag{20}$$

3. Solution approach

The governing model with boundary values is discretized using finite difference approximations. The discretization results in finite difference equations, which will be solved subsequently at distinct points within the physical domain of the model. However, it is challenging to mesh the wavy cavity with uniform spacing within the physical domain, as well as to have the grid points coincide with the boundaries of the

wavy cavity. That is, uniform spacing produces a rectangular domain, and not all the boundary grid points will coincide with the wavy boundary. Hence, a transformation from a non-rectangular, non-uniform spacing physical field to a computational field (rectangular) with uniform step size is introduced. The resulting algebraic system will map the wavy cavity from $(X,\ Y)$ system to a rectangular $(\xi,\ \eta)$ system, where:

$$\xi = \frac{X}{1 - A_w + A_w \cos\left(2\pi\lambda_w Y\right)},\ \ \eta = Y. \tag{21}$$

Using the above relations, the governing model is transformed into the computational field, and the model after performing the transformation is:

$$a\frac{\partial^2\Psi}{\partial\xi^2} + 2b\frac{\partial^2\Psi}{\partial\xi\partial\eta} + c\frac{\partial^2\Psi}{\partial\eta^2} + d\frac{\partial\Psi}{\partial\xi} + e\frac{\partial\Psi}{\partial\eta} = -Ra_D\left(\frac{\partial\xi}{\partial X}\frac{\partial\Theta}{\partial\xi} + \frac{\partial\eta}{\partial X}\frac{\partial\Theta}{\partial\eta}\right), \tag{22}$$

$$a\frac{\partial^2\Theta}{\partial\xi^2} + 2b\frac{\partial^2\Theta}{\partial\xi\partial\eta} + c\frac{\partial^2\Theta}{\partial\eta^2} + d\frac{\partial\Theta}{\partial\xi} + e\frac{\partial\Theta}{\partial\eta} = f\left(\frac{\partial\Psi}{\partial\eta}\frac{\partial\Theta}{\partial\xi} + \frac{\partial\Psi}{\partial\xi}\frac{\partial\Theta}{\partial\eta}\right), \tag{23}$$

where,

$$a = \left(\frac{\partial\xi}{\partial X}\right)^2 + \left(\frac{\partial\xi}{\partial Y}\right)^2,\ \ b = \frac{\partial\xi}{\partial X}\frac{\partial\eta}{\partial X} + \frac{\partial\xi}{\partial Y}\frac{\partial\eta}{\partial Y},\ \ c = \left(\frac{\partial\eta}{\partial X}\right)^2 + \left(\frac{\partial\eta}{\partial Y}\right)^2,$$

$$d = \frac{\partial^2\xi}{\partial X^2} + \frac{\partial^2\xi}{\partial Y^2},\ \ e = \frac{\partial^2\eta}{\partial X^2} + \frac{\partial^2\eta}{\partial Y^2},\ \ f = \frac{\partial\xi}{\partial X}\frac{\partial\eta}{\partial Y} - \frac{\partial\xi}{\partial Y}\frac{\partial\eta}{\partial X},$$

and the transformed boundary values are:

on (all) walls:

$$\Psi = 0, \tag{24a}$$

on $\xi = 0$, $(P_H/H_E\ - 1/4) \le \eta \le (P_H/H_E + 1/4)$:

$$\Theta = 1, \tag{24b}$$

on $\xi = 1$, $0 \le \eta \le 1$:

$$\Theta = 0, \tag{24c}$$

on $\xi = 0$, $0 < \eta < (P_H/H_E\ - 1/4)$ & $(P_H/H_E + 1/4) < \eta < 1$:

$$\frac{\partial\xi}{\partial X}\frac{\partial\Theta}{\partial\xi} + \frac{\partial\eta}{\partial X}\frac{\partial\Theta}{\partial\eta} = 0, \tag{24d}$$

on $\eta = 0$ & 1, $0 \le \xi \le 1$:

$$\frac{\partial\xi}{\partial Y}\frac{\partial\Theta}{\partial\xi} + \frac{\partial\eta}{\partial Y}\frac{\partial\Theta}{\partial\eta} = 0. \tag{24e}$$

The non-dimensional heat function in $(\xi,\ \eta)$ space is:

$$\begin{aligned} a\frac{\partial^2 H}{\partial\xi^2} + 2b\frac{\partial^2 H}{\partial\xi\partial\eta} + c\frac{\partial^2 H}{\partial\eta^2} + d\frac{\partial H}{\partial\xi} + e\frac{\partial H}{\partial\eta} = &\left[a\frac{\partial\Psi}{\partial\xi}\frac{\partial\Theta}{\partial\xi} + b\left(\frac{\partial\Psi}{\partial\eta}\frac{\partial\Theta}{\partial\xi} + \frac{\partial\Psi}{\partial\xi}\frac{\partial\Theta}{\partial\eta}\right) + c\frac{\partial\Psi}{\partial\eta}\frac{\partial\Theta}{\partial\eta}\right] \\ &+\Theta\left(a\frac{\partial^2\Psi}{\partial\xi^2} + 2b\frac{\partial^2\Psi}{\partial\xi\partial\eta} + c\frac{\partial^2\Psi}{\partial\eta^2} + d\frac{\partial\Psi}{\partial\xi} + e\frac{\partial\Psi}{\partial\eta}\right), \end{aligned} \tag{25}$$

with boundary values:

on $\eta = 0$ & $1, 0 \leq \xi \leq 1$:

$$H(\xi, \eta) = H(0, \eta) - \int_0^{\xi} \left(\frac{\partial \xi}{\partial Y} \frac{\partial \Theta}{\partial \xi} + \frac{\partial \eta}{\partial Y} \frac{\partial \Theta}{\partial \eta} \right) \quad \mathrm{d}\xi, \tag{26a}$$

on $\xi = 0$ & $1, 0 \leq \eta \leq 1$:

$$H(\xi,\ \eta) = H(\xi, 0) - \int_0^{\eta} \frac{1}{f} \left[\frac{\partial \xi}{\partial X} \cos(\phi) - \frac{\partial \xi}{\partial Y} \sin(\phi) \right] \frac{\partial \Theta}{\partial N} \quad \mathrm{d}\eta, \tag{26b}$$

where ϕ is the inclination of the sidewall from the y-axis, that is, $\phi = 0^{\circ}$ for left sidewall computation.

Also, the Nusselt numbers in the computational coordinate structure are calculated as:

$$Nu = -\left[\frac{\partial \Theta}{\partial \xi} \left(\frac{\partial \xi}{\partial X} \cos(\phi) - \frac{\partial \xi}{\partial Y} \sin(\phi) \right) + \left(\frac{\partial \eta}{\partial X} \cos(\phi) - \frac{\partial \eta}{\partial Y} \sin(\phi) \right) \frac{\partial \Theta}{\partial \eta} \right], \tag{27}$$

$$\overline{Nu} = 2 \int_{\frac{P_H}{H_E} - \frac{1}{4}}^{\frac{P_H}{H_E} + \frac{1}{4}} \frac{1}{J} \frac{\partial \xi}{\partial X} Nu \, d\eta, \tag{28}$$

Where,

$$J = \frac{1}{\frac{\partial X}{\partial \xi} \frac{\partial Y}{\partial \eta} - \frac{\partial X}{\partial \eta} \frac{\partial Y}{\partial \xi}}$$

is the Jacobian.

Using the finite difference technique, the altered governing Equations (22), (23) and (25), as well as the associated boundary conditions (24) and (26), are now discretized. Boundary values are approximated using 2nd-order forward and backward schemes, whereas interior points are approximated using the 2nd-order central difference method. The stream function Equation (22), energy Equation (23), and heat function Equation (25), are all iteratively solved by the Successive-Under-Relaxation (SUR) method. The equations are solved until the subsequent convergence condition is satisfied, which is:

$$\varepsilon = \max_{i,j} \left| {\varsigma_{i,j}}^{(n+1)} - {\varsigma_{i,j}}^{(n)} \right| < 10^{-6}, \tag{29}$$

where ς is either Θ or Ψ, "i" and "j" give discrete points in the $(\xi,\ \eta)$ coordinate system, and "(n)" refers to the iteration number. The average Nusselt number is calculated using the Trapezoidal rule.

Uniform-sized grids in the η- and ξ-directions are utilised for all calculations. A grid test was completed before all computations to select an appropriate grid size for future simulations. The averaged Nusselt number along the heated wall was used as a measurement for the grid-independent examination. The test was completed for square ($\lambda_w = A_w = 0$) and wavy ($\lambda_w = 5,\ A_w = 0.25$) cavities at $Ra_D = 10^3$. The results in **Table 1** show that the grid size 150×200 is suitable for calculations, as it performed as well as finer meshes considered for the grid test carried out in the range of 80×80 to 200×200 grids. The results in **Table 2** verified the numerical code of the present study with the literature available for a differentially heated Darcy-porous square cavity.

The decent outcomes presented provide confidence in our numerical solutions.

Table 1. Grid independence test for the differentially heated wavy and square cavities at $Ra_D = 10^3$.

Grid size	$\overline{Nu}$	
	$A_w = 0.25, \lambda_w = 5$	$A_w = 0, \lambda_w = 0$
80 × 80	14.0048	13.1219
100 × 100	14.1070	13.2800
150 × 150	14.2337	13.4507
150 × 180	14.2646	13.4630
150 × 200	14.2805	13.4692
180 × 180	14.2754	13.4966
200 × 200	14.2967	13.5175

Table 2. $\overline{Nu}$ values for buoyant convection in a porous cavity.

References	$\overline{Nu}$	
	$Ra_D = 10^2$	$Ra_D = 10^3$
Misirlioglu et al. [6]	3.050	13.150
Zhao et al. [23,24]	3.100	13.450
Mansour et al. [8]	3.207	-
Sojoudi et al. [9]	3.105	13.019
Present study	3.101	13.280

4. Discussion

Numerical simulation is used to examine natural convection streams and thermal transport in a wavy-shaped porous cavity with a localized heat source on the left sidewall. Amplitude (A_w) and undulation number (λ_w), which fall between $0 \leq A_w \leq 0.15$ and $0 \leq \lambda_w \leq 3$, respectively, control the wall's waviness. The locations of the heater (P_H) on the left wall are $H_E/4$ (lower heating), $H_E/2$ (center heating), and $3H_E/4$ (upper heating), in that order. The Ra_D, which ranges from 10 to 10^3, is utilized to judge the significance of convective heat transport. Plotting the related contours of stream function, temperature, and cavity heat function illustrates the stream pattern, thermal distribution, and heat transport in the cavity. Nusselt values, both local and average, are utilized to show the amount of heat transfer.

The impacts of the right wall's waviness and heating sites on the stream field, and thermal transport inside the wavy cavity at $Ra_D = 10^3$ are shown in the following figures. In **Figure 2**, the isotherms unequivocally demonstrate how the heat source location influences the cavity's thermal distribution. The isotherms are found to be grouped around the heater in every instance of the heating site. The establishment of a thermal boundary layer and the presence of sharp thermal gradients in a horizontal direction along the heater are both suggested by the gathering of isotherms. Additionally, the isotherms accumulated at the upper right wall, indicating that a thermal boundary layer had formed along the right wall's upper-right corner. Convective movement from the heat source to the right wall at $Ra_D = 10^3$ is further demonstrated by the spreadable isotherms, which show the thermal stratification in

the cavity from bottom to top. The temperature layers are evenly spread throughout the cavity when lower heating is supplied to the left wall. When the heating location is changed to center heating, cold fluid occupies the bottom sector of the chamber exclusively, and thermal stratification starts from one-quarter (where the heater's leading edge is located). Since the lower portion of the cavity is occupied with cold fluid and the upper part of the cavity is occupied by thermal stratification, the same effect can be seen in the upper-heating scenario. As a result, changes in the heating position from lower to upper have an impact on the thermal spreading within the hollow, and the region of cold fluid in the lower part of the cavity grows. Furthermore, the span of the thermal (boundary) layer near the right sidewall is influenced by the heating sites; when bottom heating is used, the thermal layer extends from the upper part to the middle of the right sidewall, whereas the extension is shorter when upper heating is used.

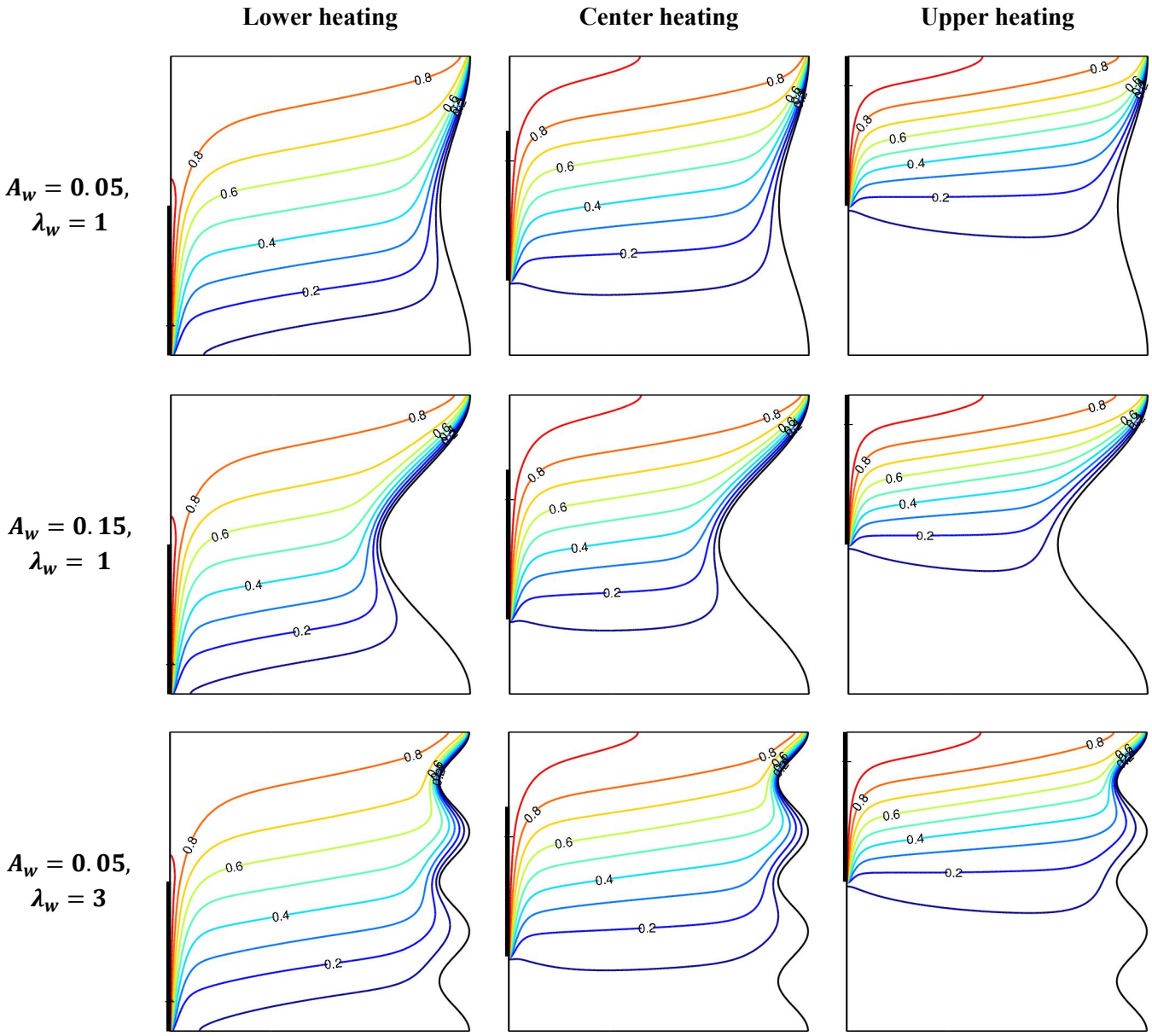

Figure 2. *Cont.*

$A_w = 0.15$,
$\lambda_w = 3$

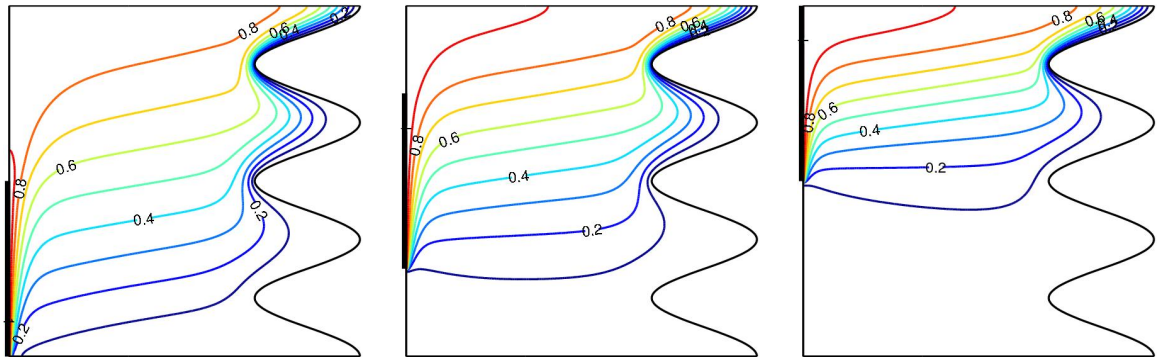

Figure 2. Isotherms for a porous cavity with different heating locations (upper, center and lower heating), amplitudes ($A_w = 0.05$ and 0.15) and undulations ($\lambda_w = 1$ and 3) at $Ra_D = 10^3$.

Additionally, **Figure 2** shows that the thermal circulation in the wavy cavity is influenced by the right sidewall's waviness. A wavy thermal boundary layer with bunched isotherms forms along the right wall as a result of the right sidewall's wavy nature. The thermal boundary layer extends from the upper-right corner, and as the amplitude rises, so does its length, increasing the wavy wall's arc length. The top-most undulation is always the initial zone of experience for heat energy exchange because heat exchange always occurs at the top of the right wall when hot fluid from the left wall approaches the cold wall. In comparison to the thermal layer near the right wall, which has more waves, it looks to be shorter. As a result, the thermal distribution at the right sidewall is mostly influenced by its waviness.

Streamlines in **Figure 3** demonstrate that when the lower heating case, the entire cavity is filled with clockwise circulating flow. Fluid particles next to the heater are continuously heated and finally get activated when the heater is at the bottom. Particles of energized fluid start to rise along the wall because they are less dense. There is no horizontal energy exchange between the fluid particles and the left wall. The liquid particles get denser and then sink near the cold right wall when the hot fluid approaches the cool right wall, losing energy in the process. Thus, the cavity exhibits a clockwise circulating flow. The streamlines cluster along the heater when center and upper heating are applied, indicating the formation of the momentum boundary layer and consistent with the creation of the thermal boundary layer seen in **Figure 2**. Because the lower part of the cavity is occupied with cold fluid, flow is stationary in the region under the heater's leading edge. The heater's position on the left wall determines the rotation of the main core of the circulating flow, and when the heater's position changes from lowest to upper, the circulation strength decreases.

Figure 3 illustrates that for a fixed undulation, a larger amplitude of the waviness produces a smaller main core stream. The stream is restricted by the high amplitude of wavy walls because it condenses the cavity's space. However, a greater undulation number affects the stream field when the cavity has the same amplitude, since the main stream is larger while there are more undulations. The velocity boundary layer is visible near the right wall. It is also parallel to the temperature boundary layer shown in **Figure 2**. More undulations in the wavy wall result in a shorter momentum boundary layer

from the right-top region. The bottom region is close to undulations, also experiencing fluid stagnation. This is because stream motion is too minimal in the lower-half of the undulating right wall due to the dense and low-energy nature of the fluid particles.

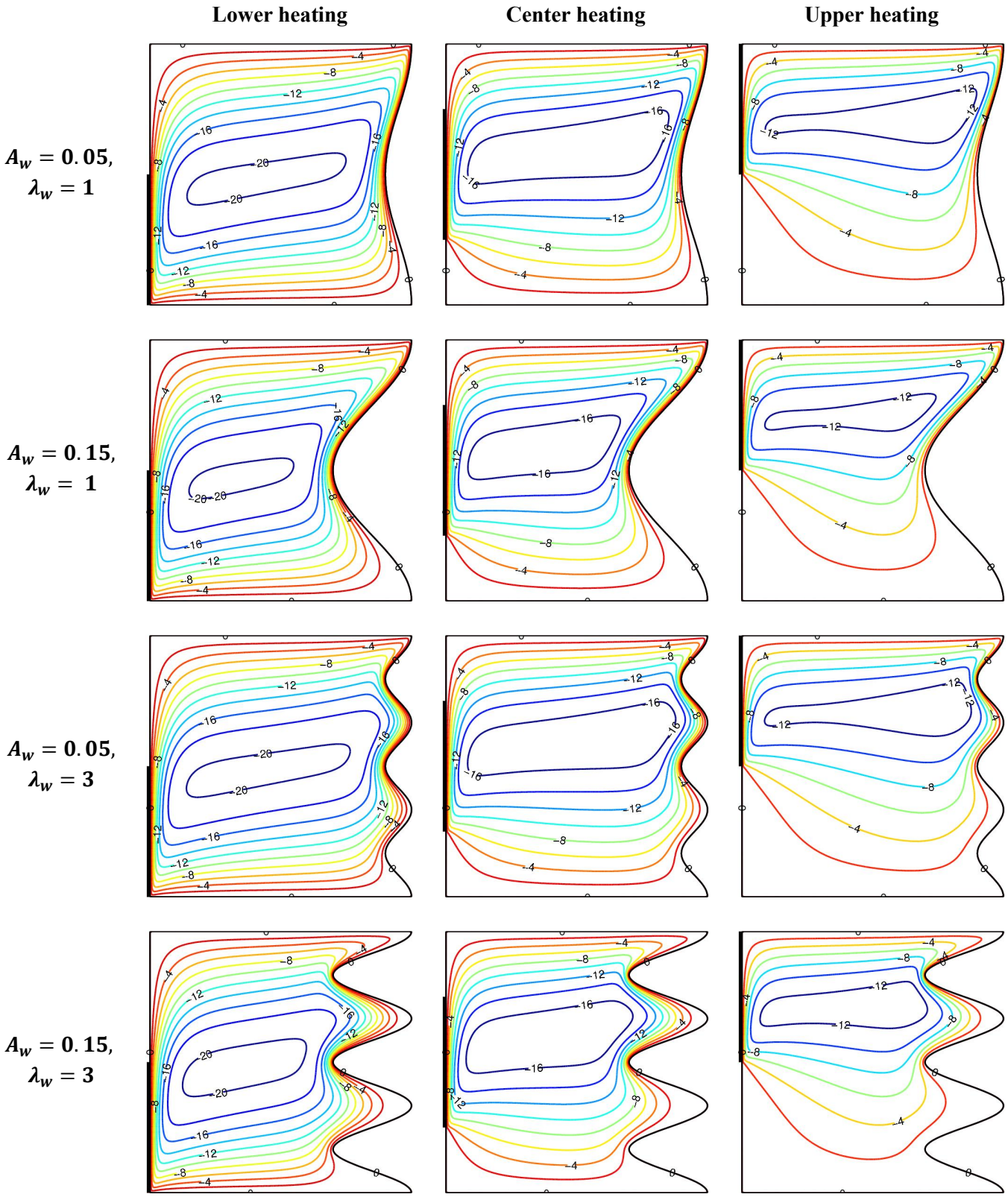

Figure 3. Streamlines for a porous cavity with different heating locations (upper, center and lower heating), amplitudes ($A_w = 0.05$ and 0.15) and undulations ($\lambda_w = 1$ and 3) at $Ra_D = 10^3$.

Heatlines in **Figure 4** demonstrate the impact of heater location(s) on heat transport inside the wavy porous cavity. The heatlines are protracted from the source to the cold right wall, indicating that heat is transferred from the heater to the cold wall. It can be detected from the center and upper heating cases that heat transport starts from the leading edge of the heat source. The heatlines are then stretched from the heat source to the colder side, and end at the right-top region, indicating the occurrence of high heat transport at the top-right edge of the porous chamber. The direction of heat transport of the main core is the same as the fluid flow. This is because the convective current is more prominent at $Ra_D = 10^3$; hence, heat transport inside the cavity is driven by the bulk fluid motion. Other than that, the main core is adjacent to the heater, indicating that heat flow is affected by the heater position. The strength of heat transport is higher for the lower heating scenario since it has a higher strength of flow circulation inside the porous cavity, as presented in **Figure 3**. However, heat flow intensity is low in the center heating scenario. It is noted that heat transport is low in areas below the leading edge of the source. Isotherms in **Figure 2** reveal that the fluid is cold and isothermal, indicating the domination of conductive heat transfer, and hence, heat transport is low. The waviness of the right wall affects heat transport inside the porous cavity, especially along the wavy wall. The heatlines also show that heat transmission is higher at the top hull of the wavy wall in the case of 3 undulations.

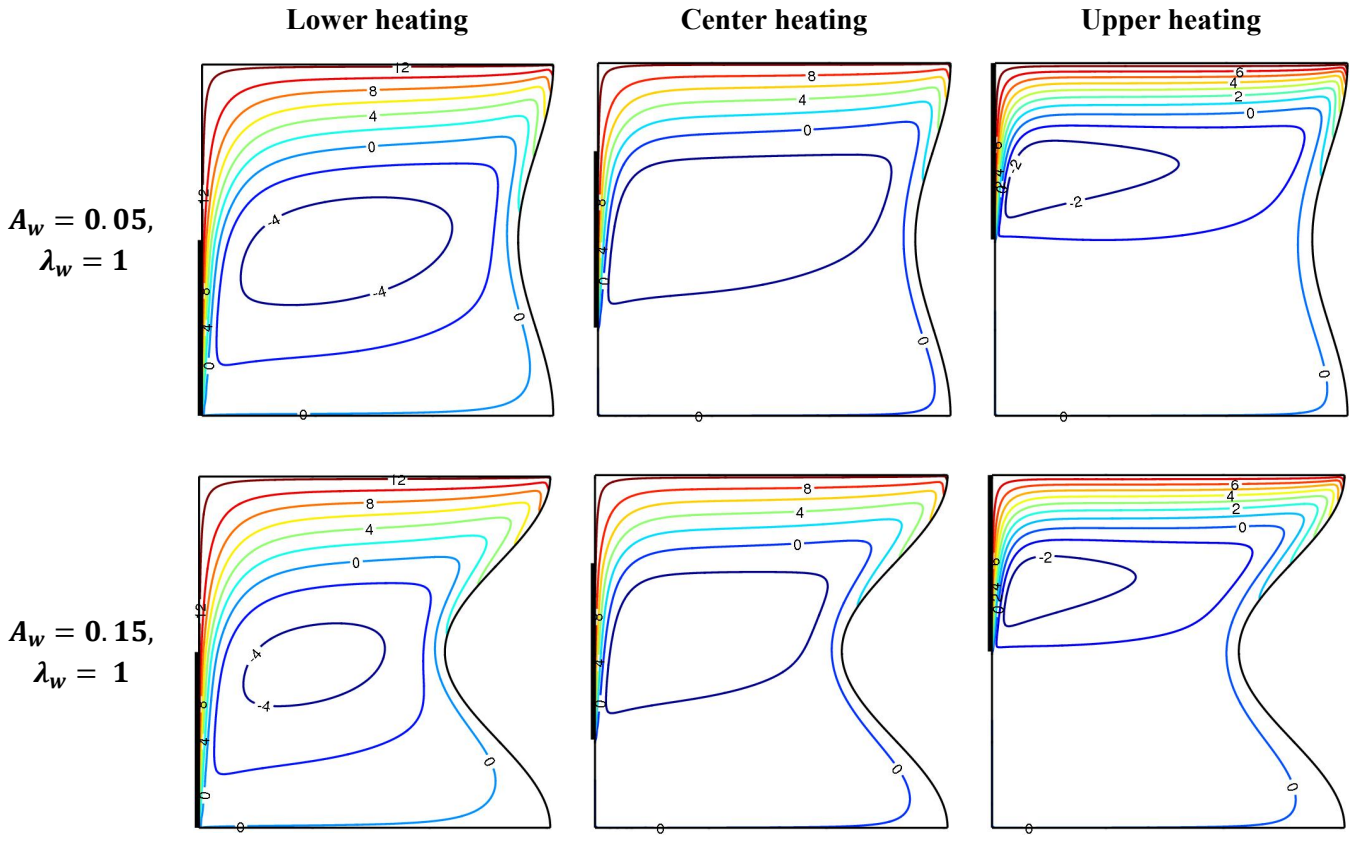

Figure 4. *Cont.*

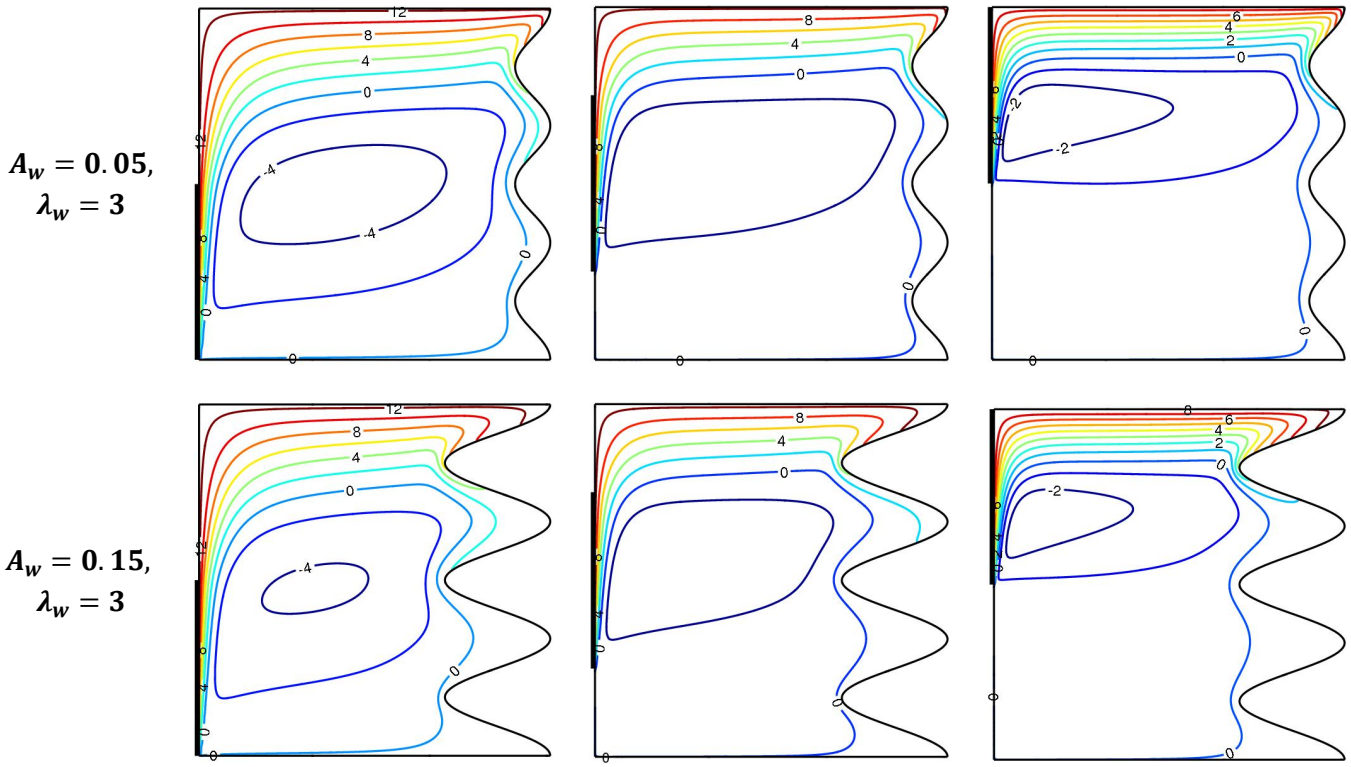

Figure 4. Heatlines for a porous cavity with different heating locations (upper, center and lower heating), amplitudes ($A_w = 0.05$ and 0.15) and undulations ($\lambda_w = 1$ and 3) at $Ra_D = 10^3$.

Figure 5 displays the local thermal energy transport rate along the cavity's left and right sidewalls. It is evident that the heat transfer amount is drastically dropping along the heat source for the left wall. High amplitude cavities provide higher heat energy transport at the heater's foremost edge because they maintain a constant heating location and number of undulations. Additionally, as the heat source shifts from lower to upper heating, the heat energy transport rate at the heater's end reduces. The plot for the local Nu along the right wall has a wavy shape, and the undulation number on the wavy right wall equals the wave number. It is detected that the local energy transport along the right sidewall surges from the foremost edge of the right sidewall. The range of heat energy transport shrinks as the amplitude is growing, and lower heating has enhanced local heat transport along the heat source.

Figure 6 demonstrates the averaged heat transfer rates along the heater. As the Ra_D number rises, so does the rate of heat transmission. The rise of the Ra_D rises the ratio of buoyant force to viscous strength of liquid in the cavity. The decrease in viscous force between fluid particles cuts the distance between the heat source and adjacent fluid particles, and henceforth, the amount of heat passage between the source and fluid increases. Additionally, as the undulations and amplitude increase, so does the average heat transmission rate. The heat transport from the source into the chamber is accelerated by the undulating right wall's increased surface for thermal energy passage between the medium and the wall. Furthermore, compared to other heater placements, it is evident that lower heating on the left sidewall generates a higher rate of heat transmission. However, when the strength of convection is minimal, that is, at $Ra_D = 10$, center heating results in a larger amount of energy transfer than

other sites of heater. Fluid is circulating in the hollow as a result of bottom heating, which causes fluid motion from the wall's bottom. When fluid is flowing along the heat source, a higher rate of heat transfer can be accomplished because higher Ra_D lowers fluid viscosity. Diffusion will be the cavity's heat transfer mechanism, fluid viscosity is high, and center heating effectively encourages fluid mixing in the cavity when the Ra_D is low.

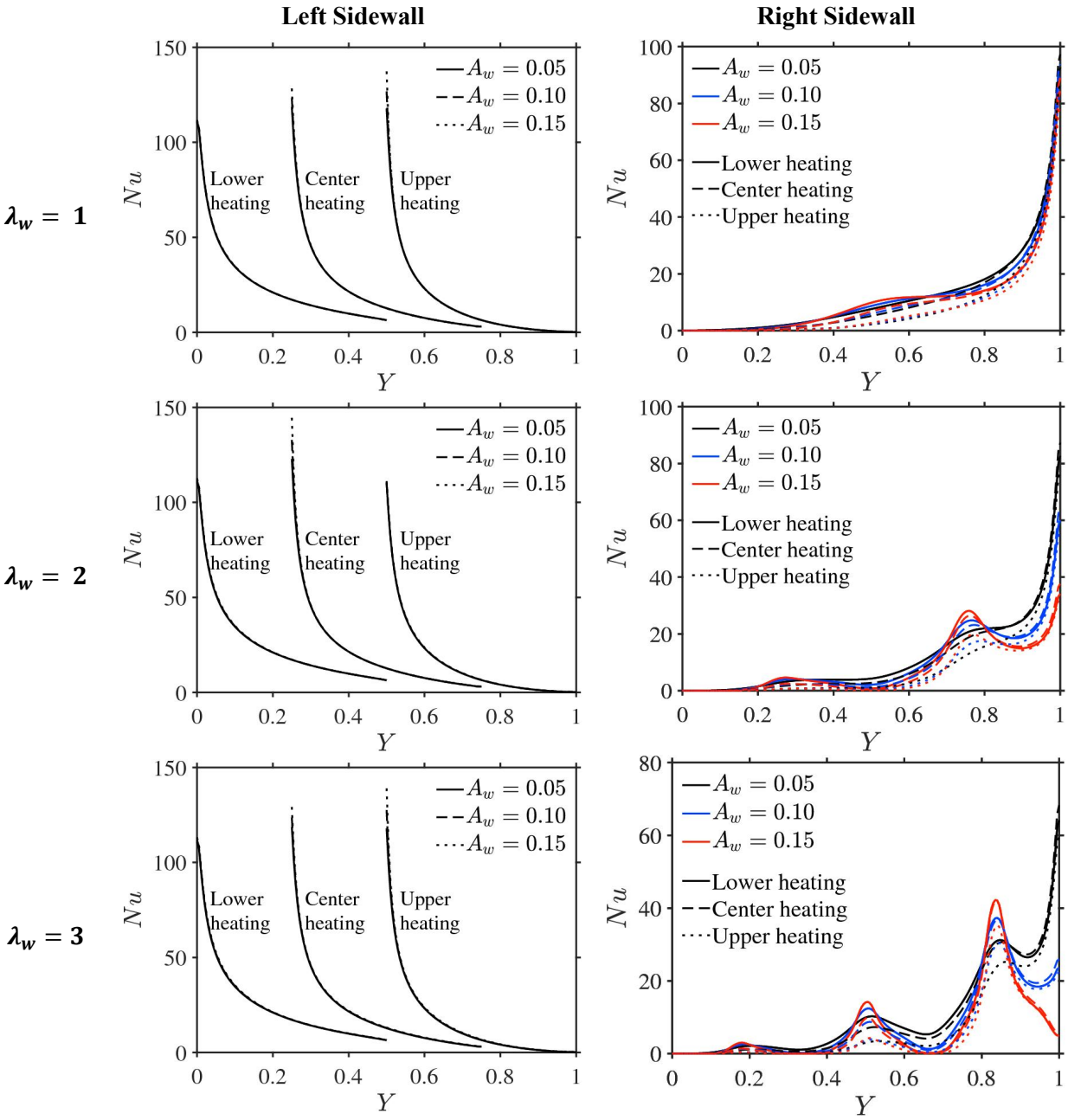

Figure 5. Local Nusselt numbers along the left and right sidewalls for various heating locations (lower, center, and upper heating) and waviness of the right sidewall ($\lambda_w = 1$, 2, and 3) at $Ra_D = 10^3$.

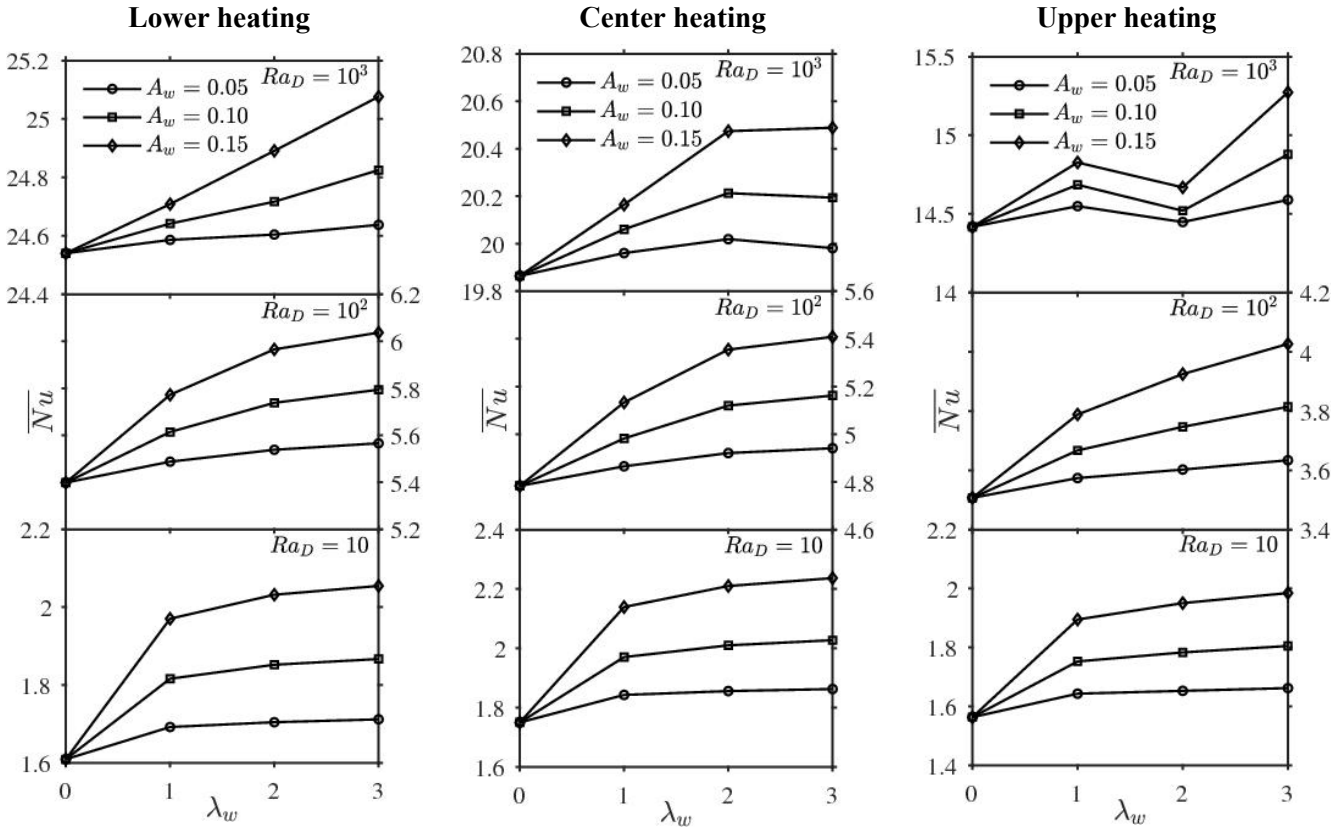

Figure 6. The average Nusselt number versus the number of undulations (λ_w) for various amplitudes (A_w), Ra_D and heating locations.

For a better visualization of the enhancement of heat transmission for different heater locations and the right-side wall's waviness, **Table 3** shows the averaged Nusselt number on the left sidewall with comparison between the wavy and square cavities. It can be observed that the heat transfer rate increases with increased amplitude and undulation number for lower heating, but center and upper heating do not consistently show the same trend; center heating with 3 undulations has slightly lower heat transfer rates compared to 2 undulations, whereas upper heating with 2 undulations has lower heat transfer rates compared to 1 and 3 undulations. This trend is an unexpected finding in the present study, and further investigation, whether on the governing system or real-life cases, is needed to justify the finding. On the overall trend, lower heating shows 84.79% performance enhancements compared with a differentially heated square cavity ($H_E = 1$, $\overline{Nu} = 13.280$ as recorded in **Table 2**), followed by center and upper heating, with enhancement of 49.58% and 8.57%, respectively.

The relationships between the $\overline{Nu}$ and the parameters taken into consideration in this study and the data collected are provided by correlation equations that are developed from the numerical data. The $\overline{Nu}$ for a square cavity with a set span of heater $\frac{H_E}{2}$ situated at various positions on the left sidewall can be calculated as follows:

$$\overline{Nu} = 2\left[\frac{1 + 0.0460{Ra_D}^{0.71}}{\left(\frac{\mathrm{P}_H}{H_E}\right)^2 - 0.194\left(\frac{\mathrm{P}_H}{H_E}\right) + 0.507} - 1.535\left(\frac{\mathrm{P}_H}{H_E}\right)^2 + 3.469\left(\frac{\mathrm{P}_H}{H_E}\right) - 2.335\right],$$

with goodness-of-fit of R-squared and adjusted R-squared of 0.99.

The $\overline{Nu}$ is found to vary inconsistently with Ra_D, heater places, and the right wall's waviness.

Table 3. Averaged Nusselt numbers on the left sidewall for various undulation numbers, amplitude, and heating locations at $Ra_D = 10^3$, with comparisons on the change of $\overline{Nu}$ with a square porous cavity ($A_w = 0.00$, $\lambda_w = 0$).

A_w	λ_w	Lower heating		Center heating		Upper heating	
		$\overline{Nu}$	% change	$\overline{Nu}$	% change	$\overline{Nu}$	% change
0.00	0	24.5407	-	19.8642	-	14.4180	-
0.05	1	24.5864	0.19	19.9604	0.48	14.5495	0.91
	2	24.6047	0.26	20.0191	0.78	14.4485	0.21
	3	24.6379	0.40	19.9812	0.59	14.5897	1.19
0.10	1	24.6421	0.41	20.0605	0.99	14.6854	1.85
	2	24.7172	0.72	20.2128	1.75	14.5202	0.71
	3	24.8252	1.16	20.1938	1.66	14.8782	3.19
0.15	1	24.7088	0.68	20.1642	1.51	14.8272	2.84
	2	24.8913	1.43	20.4740	3.07	14.6687	1.74
	3	25.0764	2.18	20.4884	3.14	15.2737	5.93

5. Conclusion

Numerical research was done on natural convective motion in a wavy-shaped porous chamber with localized heating. The stream and thermal distribution within the hollow are impacted by the heater's placement on the left wall. Additionally, the cavity's temperature and flow are impacted by the right sidewall's waviness, particularly along the right-sided wavy wall. The circulating current is shown to be clockwise independent of the heater position. On the other hand, the placement of the convective cell's core region is influenced by heating locations. The heater's leading edge has a high heat transfer rate, whereas the heater's end has a low heat transmission rate. It has been found that the right sidewall's waviness increases the pace at which heat transfers into the cavity. When convection intensity is high, lower heating results in the greatest heat transfer into the cavity; for example, $Ra_D \geq 10^2$. Heat transport into the cavity is improved by middle heating for low Darcy–Rayleigh number ($Ra_D = 10$). This study is important to provide insight into the thermal design of porous systems involving non-uniform heating, such as solar air conditioning, ventilation, and heating systems.

Author contributions: Conceptualization, SS; methodology, HTC and SS; software, HTC and SS; validation, HTC and SS; formal analysis, HTC and SS; investigation, HTC and SS; writing—original draft preparation, HTC and SS; writing—review and editing, SS; visualization, HTC and SS; supervision, SS. All authors have read and agreed to the published version of the manuscript.

Funding: No funding is received for this research.

Institutional review board statement: Not applicable.

Informed consent statement: Not applicable.

Data availability statement: No data is generated.

Conflict of interest: The authors declare no conflict of interest.

AI use statement: During the preparation of this manuscript, the authors used Turnitin solely for language refinement. No AI tools were used for data analysis, interpretation, or generation of scientific content. All outputs were critically reviewed and edited by the authors. The authors take full responsibility for the integrity and accuracy of the work.

Abbreviations

A_w	Amplitude
c_P	Specific heat capacity
g	Gravitational acceleration
h	Heat function
H	Dimensionless heat function
k	Thermal conductivity
K	Porous medium permeability
H_E	Width/height of the cavity
n, s	Normal and tangent planes
N, S	Dimensionless normal and tangent
Nu	Nusselt number
$\overline{Nu}$	Average Nusselt number
P	Pressure
P_H	Position of the heater
q	Heat transfer rate
$\bar{q}$	Average heat transfer rate
Ra_D	Darcy–Rayleigh number
T	Temperature
u, v	Velocity in x- and y-directions
x, y	Cartesian coordinates
X, Y	Dimensionless Cartesian coordinates

Greek symbols

α	Thermal diffusivity
β	thermal expansion coefficient
λ_w	Number of undulations
μ	Viscosity
υ	Kinematic viscosity
ψ	Stream function
Ψ	Dimensionless stream function
ρ	Density
Θ	Dimensionless temperature
ξ, η	Computational space coordinates

Subscripts

C	Cold
H	Hot

References

1. Upreti H, Pandey A, Gupta T. Exploring the Flow Dynamics of MHD Hybrid Nanofluid over a Non-Flat Porous Surface Using Neural Network Approach. Revista Internacional de Métodos Numéricos para Cálculo y Diseño en Ingeniería. 2025; 41(2). doi: 10.23967/j.rimni.2025.10.64380
2. Sharma PK, Sharma BK, Kumar A. Mathematical Analysis of Chemically Reacting Species and Radiation Effects on MHD Free Convective Flow Through a Rotating Porous Medium. Acta Mechanica et Automatica. 2024; 18(2): 193–203. doi: 10.2478/ama-2024-0023
3. Murthy PVSN, Kumar BVR, Singh P. Natural Convection Heat Transfer from a Horizontal Wavy Surface in a Porous Enclosure. Numerical Heat Transfer, Part A: Applications. 1997; 31(2): 207–221. doi: 10.1080/10407789708914033
4. Rathish Kumar BV, Shalini. Free convection in a non-Darcian wavy porous enclosure. International Journal of Engineering Science. 2003; 41(16): 1827–1848. doi: 10.1016/S0020-7225(03)00113-7
5. Das PK, Mahmud S, Humaira Tasnim S, et al. Effect of surface waviness and aspect ratio on heat transfer inside a wavy enclosure. International Journal of Numerical Methods for Heat & Fluid Flow. 2003; 13(8): 1097–1122. doi: 10.1108/09615530310501975
6. Misirlioglu A, Baytas AC, Pop I. Free convection in a wavy cavity filled with a porous medium. International Journal of Heat and Mass Transfer. 2005; 48(9): 1840–1850. doi: 10.1016/j.ijheatmasstransfer.2004.12.005
7. Chen XB, Yu P, Winoto SH, et al. Free Convection in a Porous Wavy Cavity Based on the Darcy-Brinkman-Forchheimer Extended Model. Numerical Heat Transfer, Part A: Applications. 2007; 52(4): 377–397. doi: 10.1080/10407780701301595
8. Mansour MA, El-Aziz MMA, Mohamed RA, et al. Numerical Simulation of Natural Convection in Wavy Porous Cavities Under the Influence of Thermal Radiation Using a Thermal Non-equilibrium Model. Transport in Porous Media. 2011; 86(2): 585–600. doi: 10.1007/s11242-010-9641-5
9. Sojoudi A, Saha SC, Khezerloo M, et al. Unsteady Natural Convection Within a Porous Enclosure of Sinusoidal Corrugated Side Walls. Transport in Porous Media. 2014; 104(3): 537–552. doi: 10.1007/s11242-014-0347-y
10. Prakash O, Barman P, Rao PS, et al. MHD free convection in a partially open wavy porous cavity filled with nanofluid. Numerical Heat Transfer, Part A: Applications. 2023; 84(5): 449–463. doi: 10.1080/10407782.2022.2132330
11. Armaghani T, Rashad AM, Togun H, et al. Hybrid Nanofluid Unsteady MHD Natural Convection in an Inclined Wavy Porous Enclosure with Radiation Effect, Partial Heater and Heat Generation/Absorption. Iranian Journal of Science and Technology, Transactions of Mechanical Engineering. 2024; 48(3): 971–988. doi: 10.1007/s40997-023-00720-3
12. Tanveer A, Sami-ul-Haq, Ashraf MB, et al. Thermal analysis of nonlinear mixed convection effects within wavy enclosure. Case Studies in Thermal Engineering. 2024; 63: 105322. doi: 10.1016/j.csite.2024.105322
13. Chuhan IS, Li J, Guo Z, et al. Entropy optimization of MHD non-Newtonian fluid in a wavy enclosure with double diffusive natural convection. Numerical Heat Transfer, Part A: Applications. 2024; 85(16): 2703–2723. doi: 10.1080/10407782.2023.2228482
14. Mandal DK, Mondal MK, Biswas N, et al. Convective heat transport in a porous wavy enclosure: Nonuniform multi-frequency heating with hybrid nanofluid and magnetic field. Heliyon. 2024; 10(9): e29846. doi: 10.1016/j.heliyon.2024.e29846
15. Sivasankaran S, Cheong HT, Aasaithambi T. Effect of Localized Heater Position and Length on Buoyant Convection in an Oblique Porous cavity Using Heatlines Approach. International Journal of Applied and Computational Mathematics. 2025; 11(5): 181. doi: 10.1007/s40819-025-01996-6
16. Hansda S, Majhi D, Hussein AK, et al. Magento-double diffusive natural convection in a partially heated wavy porous cavity filled with a radiative hybrid nanofluid. Journal of Thermal Analysis and Calorimetry. 2025; 150(13): 10489–10512. doi: 10.1007/s10973-025-14398-z
17. Parmar D, Murthy SVSSNVGK, Kumar BVR, et al. Numerical simulation of fractional order double diffusive convective nanofluid flow in a wavy porous enclosure. International Journal of Heat and Fluid Flow. 2025; 112: 109749. doi: 10.1016/j.ijheatfluidflow.2025.109749
18. Barman P, Kumar BVR. FEA of entropy generation due to free convection of hybrid-nanofluid in a partially heated tilted porous enclosure with wavy wall. International Journal of Numerical Methods for Heat & Fluid Flow. 2025; 35(9): 3029–3052. doi: 10.1108/HFF-09-2024-0723
19. Roy NC, Rumpa SH, Amin A. Natural convective ternary nanofluid flow in a trapezoidal wavy enclosure with multiple cold obstacles. International Journal of Heat and Fluid Flow. 2026; 117: 110139. doi:

10.1016/j.ijheatfluidflow.2025.110139
20. Sankar M, Bhuvaneswari M, Sivasankaran S, et al. Buoyancy induced convection in a porous cavity with partially thermally active sidewalls. International Journal of Heat and Mass Transfer. 2011; 54(25–26): 5173–5182. doi: 10.1016/j.ijheatmasstransfer.2011.08.029
21. Sivasankaran S, Bhuvaneswari M. Effect of thermally active zones and direction of magnetic field on hydromagnetic convection in an enclosure. Thermal Science. 2011; 15: 367–382. doi: 10.2298/TSCI100221094S
22. Chen TH, Chen LY. Study of buoyancy-induced flows subjected to partially heated sources on the left and bottom walls in a square enclosure. International Journal of Thermal Sciences. 2007; 46(12): 1219–1231. doi: 10.1016/j.ijthermalsci.2006.11.021
23. Zhao FY, Liu D, Tang GF. Free convection from one thermal and solute source in a confined porous medium. Transport in Porous Media. 2007; 70(3): 407–425. doi: 10.1007/s11242-007-9106-7
24. Zhao FY, Liu D, Tang GF. Natural convection in a porous enclosure with a partial heating and salting element. International Journal of Thermal Sciences. 2008; 47(5): 569–583. doi: 10.1016/j.ijthermalsci.2007.04.006
25. Sivasankaran S, Do Y, Sankar M. Effect of Discrete Heating on Natural Convection in a Rectangular Porous Enclosure. Transport in Porous Media. 2011; 86(1): 261–281. doi: 10.1007/s11242-010-9620-x
26. Sivakumar V, Sivasankaran S, Prakash P, et al. Effect of heating location and size on mixed convection in lid-driven cavities. Computers & Mathematics with Applications. 2010; 59(9): 3053–3065. doi: 10.1016/j.camwa.2010.02.025
27. Malleswaran A, Sivasankaran S, Bhuvaneswari M. Effect of heating location and size on MHD mixed convection in a lid-driven cavity. International Journal of Numerical Methods for Heat & Fluid Flow. 2013; 23(5): 867–884. doi: 10.1108/HFF-04-2011-0082
28. Sivasankaran S, Sivakumar V, Hussein AK, et al. Mixed Convection in a Lid-Driven Two-Dimensional Square Cavity with Corner Heating and Internal Heat Generation. Numerical Heat Transfer, Part A: Applications. 2014; 65(3): 269–286. doi: 10.1080/10407782.2013.826017
29. Malleswaran A, Sivanandam S. A Numerical Simulation on MHD Mixed Convection in a Lid-driven Cavity with Corner Heaters. Journal of Applied Fluid Mechanics. 2016; 9(1): 311–319. doi: 10.18869/acadpub.jafm.68.224.22903
30. Öztop HF, Estellé P, Yan WM, et al. A brief review of natural convection in enclosures under localized heating with and without nanofluids. International Communications in Heat and Mass Transfer. 2015; 60: 37–44. doi: 10.1016/j.icheatmasstransfer.2014.11.001
31. Rao PS, Barman P. Natural Convection in an Open and Wavy Porous Cavity Submitted to a Partial Heat Source. International Journal of Applied and Computational Mathematics. 2024; 10(5): 153. doi: 10.1007/s40819-024-01782-w
32. Tharapatla G, Rajakumari P, Reddy RGV. Heat and mass transfer effects on MHD non-Newtonian fluids flow through an inclined thermally-stratified porous medium. World Journal of Engineering. 2023; 20(1): 117–130. doi: 10.1108/WJE-02-2021-0099
33. Aastha A, Chand K. Soret and Dufour Effects on Chemically Reacting and Viscous Dissipating Nanofluid Flowing Past a Moving Porous Plate in the Presence of a Heat Source/Sink. Acta Mechanica et Automatica. 2023; 17(2): 263–271. doi: 10.2478/ama-2023-0030